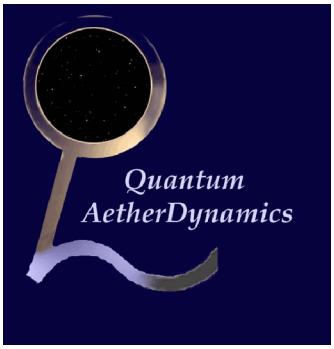


**Quantum AetherDynamics Institute (QADI)**

# The Relational Geometry of the Aether Fabric

## Six-Port Chronogeometric Closure, Particle-Mass Balance, and Discrete Compatibility Propagation

David W. Thomson III
**Quantum AetherDynamics Institute (QADI)**, Alma, Illinois, USA
ORCID: 0000-0002-5830-5427

Version 1.0 – July 25, 2026

This article is published by the Quantum AetherDynamics Institute (QADI).

It develops the Aether Physics Model (APM)

**Abstract**

The Aether Physics Model requires persistent space to be more than an undifferentiated continuum: it must be a discrete compatibility fabric whose primitive Aether Units possess internal chronogeometry, external orientation capacity, and relational packing structure. This paper develops a six-port geometry for that fabric. The starting balance condition is

$$\frac{m_p^{(0)}}{m_e} = \left(\frac{A_u}{k_C}\right)\Pi_{\text{phys}} = 16\pi^2\left(\frac{6\pi^3}{16}\right) = 6\pi^5,$$

which joins the leading proton–electron mass ratio, the Aether-unit state-space factor, and the packing invariant. Six equally phased relational components are shown to form a regular five-dimensional simplex. Antipodal parity separates its nonconstant phase space exactly into three odd spatial coordinates and two even temporal coordinates. The spatial projection yields six octahedral port normals in three antipodal pairs; the dual external compatibility cell is six-faced and supports six face-sharing nearest neighbors.

A packing-informed nearest-neighbor functional is then constructed from the logarithmic Ledger strain $\varepsilon = \ln D(\eta)$. Its variation gives a carrier-resolved graph equation for mass, electrostatic-charge, and magnetic-charge injection. The mass sector is ordered by the Primacy of Space: the spatial dynamic-domain invariant produces Keplerian orbital coherence before the Newtonian force representation. A preliminary unitary port-transfer operator preserves temporal registration while reversing the spatial normal across a shared interface. Its exact fixed-frame lattice dispersion is derived as a reciprocal sixth-degree polynomial and a reduced cubic. The long-wave propagating branch has speed $c/\sqrt{3}$, proving that a globally locked cubic frame is incomplete and that physical free propagation requires dynamical port-frame alignment and a two-state photon sector. The paper records the derived kinematic and constitutive foundation while separating completed results from open dynamics.

**Keywords:** Aether Unit; six-port geometry; discrete space; QMU; APM; loxodromic packing; particle mass; compatibility functional; force unification; photon transfer; lattice dispersion

# Contents

**1 Introduction** **4**

1.1 Scope and claim discipline . . . . . 4

**2 Aether Ontology and Ledger Prerequisites** **5**

2.1 Creation, organization, and occupation . . . . . 5

2.2 QMU identities . . . . . 6

2.3 Ledger deformation . . . . . 6

**3 Primacy of Space and the Balance Condition** **7**

3.1 The spatial dynamic-domain invariant . . . . . 7

3.2 Internal, unit-local, and relational geometry . . . . . 8

**4 From Six Packing Components to Six Relational Ports 8**

4.1 Reinterpretation of the older six-string language . . . 9

4.2 Six equal phase labels . . . 9

**5 The Regular Five-Dimensional Phase Simplex 10**

**6 Antipodal Parity and the Exact $3+2$ Split 10**

**7 Octahedral Ports and the External Compatibility Cell 11**

7.1 Exact port normals . . . 11

7.2 The dual compatibility cell . . . 12

7.3 Neighbor shells and rotational freedom . . . 13

7.4 Equal packing moments . . . 13

**8 Six-Port State Space and Projectors 13**

**9 Packing-Informed Nearest-Neighbor Compatibility 14**

9.1 Profile-level mismatch . . . 14

9.2 Small-strain coefficient . . . 15

9.3 Carrier character decomposition . . . 15

9.4 Sources and graph equation . . . 16

**10 The Three Source-Injection Laws 16**

10.1 Universal definition . . . 16

10.2 Mass injection . . . 16

10.3 Electrostatic-charge injection . . . 17

10.4 Magnetic-charge injection . . . 17

**11 Far-Field Interaction and Force Architecture 18**

11.1 Continuum Green limit . . . 18

11.2 Test response and pair energy . . . 18

11.3 Composite cancellation . . . 19

**12 Shared-Port Photon Transfer 19**

12.1 Antipodal interface rule . . . 19

12.2 Temporal phase transport . . . 20

12.3 Local unitary operator . . . . . 21

**13 Exact Fixed-Frame Lattice Dispersion** **21**

13.1 Homogeneous Bloch operator . . . . . 21

13.2 Reciprocal characteristic polynomial . . . . . 22

13.3 Natural three-registration temporal cycle . . . . . 22

13.4 Long-wave expansion and the $c/\sqrt{3}$ result . . . . . 23

13.5 Dynamical requirement . . . . . 24

**14 Predictions and Falsifiable Consequences** **24**

14.1 Balance closure . . . . . 25

14.2 Port Gram matrix . . . . . 25

14.3 Quantum-range cubic correction . . . . . 25

14.4 Frame-locked defect mode . . . . . 25

14.5 Carrier hierarchy . . . . . 25

14.6 Shared temporal registration . . . . . 25

**15 Discussion** **26**

15.1 What has been unified . . . . . 26

15.2 Why recording the fixed-frame failure matters . . . . . 26

15.3 Relation to earlier packing terminology . . . . . 26

15.4 Remaining derivations . . . . . 27

**16 Conclusion** **27**

**A Detailed Fourier-Simplex Identities** **27**

**B Port Projectors in Phase Order** **28**

**C Deformation-Series Data** **28**

**D Characteristic Polynomial Check** **29**

**E Dimensionless Numerical Bridge** **29**

**F Notation and Epistemic Ledger** **29**

# 1 Introduction

The Aether Physics Model (APM) assigns physical priority to structured space. Matter is localized organization within that structure, and force is a later material response to deformation and compatibility gradients in the surrounding Aether fabric. This ordering is inherited from the Primacy of Space program [Thomson III, 2026e]: spatial organization establishes the permitted orbital relation before a material force equation is written. The distinction parallels the historical ordering between Kepler's geometric orbital laws [Kepler, 1609, 1619] and Newton's later dynamical representation [Newton, 1687], while recasting both in the native Quantum Measurement Units (QMU) ledger.

Recent APM work has supplied three previously separate ingredients. The Aether-unit chronogeometry derives two orthogonal temporal dimensions, four available orientation states, one physically expressed occupied state, the one-state area $\lambda_C{}^2$, and the unsigned state-space factor $16\pi^2$ [Thomson III, 2026a]. The packing analysis derives a six-component loxodromic invariant

$$\Pi_{\text{phys}} = \frac{6\pi^3}{16} \tag{1}$$

and the unity product $6\pi^5$ [Thomson III, 2025d]. The particle-mass analysis independently identifies $6\pi^5$ as the leading proton–electron mass eigenvalue and supplies a finite inverse-curvature correction series [Thomson III, 2025c]. The present paper asks whether these are three unrelated uses of the same constants or three faces of a single compatibility closure.

The answer developed here is that the carrier strengths, stable-particle masses, Aether-unit geometry, and neighboring relationships are constrained by one balance condition. The six packing contributions become six relational phase components. Their five nonconstant Fourier coordinates form a regular 5-simplex. Antipodal parity then yields the exact decomposition

$$5 = 3 + 2, \tag{2}$$

with three exposed spatial coordinates and two hidden temporal coordinates. The spatial projection is an octahedral six-port frame. The octahedron is dual to a cube-like external compatibility cell, although the internal Aether geometry remains the carrier-sphere and loxodromic chronogeometry derived elsewhere [Thomson III, 2026c,a].

The paper proceeds beyond kinematics. It derives a nearest-neighbor compatibility functional, three source-injection laws, the continuum $1/r$ and inverse-square limits, and a preliminary photon-transfer operator. The exact lattice dispersion of that operator is calculated rather than assumed. The result is deliberately diagnostic: a globally fixed six-port frame produces a long-wave rate $c/\sqrt{3}$, not $c$. This failure is not hidden. It identifies the missing physical requirement—dynamical alignment of the local octahedral frame with the transported photon direction—and the need for two transverse temporal states.

Institutional attribution follows the QADI citation identity [Thomson III, 2025a]. The main text is QMU-first. Standard numerical values are used only in Appendix E to display dimensionless comparisons.

## 1.1 Scope and claim discipline

The present work makes four levels of claim.

Table 1: Status of the principal constructions.

| Status | Meaning | Examples in this paper |
|---|---|---|
| **Derived** | Follows algebraically from stated definitions and the six equal phases. | Regular 5-simplex Gram matrix; $3+2$ parity split; octahedral port Gram matrix; projector decomposition; characteristic polynomial. |
| **Constitutive selection** | Minimal QMU-consistent closure chosen where geometry does not yet uniquely select dynamics. | Squared logarithmic mismatch; linear source work; 120° temporal update; preliminary photon coupling. |
| **Open** | Requires a further geometric or dynamical derivation. | Physical packing realization; edge stiffness; dynamical port-frame alignment; two-state photon operator; independent normalization of all source coefficients. |

The paper therefore claims a space-first chronogeometric and constitutive unification of three primitive carrier interactions. It does not claim a completed dynamical theory of all force phenomena or a final free-photon operator.

# 2 Aether Ontology and Ledger Prerequisites

## 2.1 Creation, organization, and occupation

Creation belongs to the primordial Singularity bifurcation. The bifurcation produces complementary physical dimensions and sectors, including Gforce and dark matter, and electrostatic charge and magnetic charge. Gforce acting upon magnetic charge constructs the Aether Unit. The Aether Unit does not create matter. It is the non-material organizing rmfd chronogeometry that arranges the dimensions produced by the bifurcation and provides the container in which a Ligamen Circulatus may be captured and expressed as visible matter.

The two carrier spheres are complementary electrostatic-charge sectors of one primitive Aether Unit. They are not particles. Loxodromic channels are distributed magnetic-charge geometry. A Ligamen Circulatus supplies material mass geometry when one channel is occupied.

**Magnetic-charge ontology.** In this work, magnetic charge denotes the distributed loxodromic charge geometry of the Aether Unit. It is not a point-like particle, an isolated monopole, or a separately liberated material species. The signed magnetic source measure records the participation of this distributed geometry in neighboring Aether compatibility. The full temporal phase cell represents one complete double-loxodrome orientation state with physical area

$$A_A = {\lambda_C}^2. \tag{3}$$

Four $\mathbb{Z}_2 \times \mathbb{Z}_2$ orientation states are available, each with area capacity ${\lambda_C}^2$ and angular measure $4\pi^2$, but only one state is occupied and physically expressed at an exposed moment [Thomson III, 2026a].

This immediately rules out three misleading interpretations:

$$\begin{aligned} N_s = 6 &\neq \text{six simultaneously occupied Ligamen channels,} \\ \text{six ports} &\neq \text{six physical portions of one Aether surface,} \\ \text{temporal branches} &\neq \text{separate physical sheets.} \end{aligned} \tag{4}$$

The antipodal translation of the temporal chart is a symmetry within one identified cell. It does not split the Aether Unit into physically simultaneous sheets. In this paper the word *sheet* is reserved, when unavoidable, for a coordinate or integration chart. The physical terms are *orientation state*, *carrier branch*, *loxodromic channel*, *swept band*, and *compatibility port*.

## 2.2 QMU identities

The base ledger used here is

$$\{m_{\mathrm{e}}, \lambda_C, F_q, e^2, {e_{\mathrm{emax}}}^2\} = \{m_{\mathrm{e}}, \lambda_C, F_q, e^2, {e_{\mathrm{emax}}}^2\}. \tag{5}$$

The principal closures are

$$A_u \equiv \mathrm{rmfd}, \qquad A_u\,\mathrm{curl} = {F_q}^2\,{\lambda_C}^2, \qquad F_q\lambda_C = c, \tag{6}$$

and therefore

$$A_u \mathrm{curl} = \mathrm{temp} = c^2. \tag{7}$$

Here curl is the QMU scalar curl unit, not the vector operator $\boldsymbol{\nabla}\times$. The associated identities used below are

$$\mathrm{curl} = \frac{1}{\mathrm{mchg}\,\ell_L} = \frac{{e_{\mathrm{emax}}}^2}{m_{\mathrm{e}}\lambda_C}, \qquad \mathrm{mchg} = \frac{m_{\mathrm{e}}}{{e_{\mathrm{emax}}}^2}, \tag{8}$$

with the baseline Ligamen length $\ell_L = \lambda_C$, and

$$\mathrm{enrg} = m_{\mathrm{e}}{\lambda_C}^2{F_q}^2 = \frac{A_u {e_{\mathrm{emax}}}^2}{\lambda_C}. \tag{9}$$

The electric–magnetic geometric projection is

$$\frac{A_u}{k_C} = 16\pi^2, \tag{10}$$

while the elementary charge-strength relation is

$$e^2 = 8\pi\alpha {e_{\mathrm{emax}}}^2. \tag{11}$$

Equation (10) is a state-space geometry; Equation (11) is a carrier-strength relation. They must not be merged into one unnamed suppression factor [Thomson III, 2025e, 2026b].

## 2.3 Ledger deformation

The first deformation mode of the finite loxodromic channel is

$$\phi_{\xi,\eta}(\theta) = \xi\left[2\theta + \eta\sin(2\theta)\right], \qquad |\eta| < 1, \tag{12}$$

with arc density

$$g_\eta(\theta) = \sqrt{1 + 4\sin^2\theta\,[1 + \eta\cos(2\theta)]^2}. \tag{13}$$

The normalized arc response is

$$D(\eta) = \frac{\displaystyle\int_0^\pi g_\eta(\theta)\,\mathrm{d}\theta}{2E(-4)}, \tag{14}$$

where $E$ is the complete elliptic integral of the second kind. The Ledger response is

$$\frac{\mathrm{curl}}{\mathrm{curl}_0} = \frac{\bar{\ell}_{L0}}{\bar{\ell}_L} = \frac{A_{u0}}{A_u} = D(\eta). \tag{15}$$

The additive strain variable is therefore

$$\varepsilon := \ln D(\eta) = \ln\left(\frac{\mathrm{curl}}{\mathrm{curl}_0}\right) = -\ln\left(\frac{A_u}{A_{u0}}\right). \tag{16}$$

The logarithm is essential: multiplicative Ledger changes become additive across neighboring units.

# 3 Primacy of Space and the Balance Condition

## 3.1 The spatial dynamic-domain invariant

The primitive space invariant is

$$\mathrm{dtrd} = \mathrm{volm}\,\mathrm{rson} = \lambda_C{}^3 F_q{}^2 = \lambda_C c^2. \tag{17}$$

The Aether maximum mass is

$$m_a = \frac{\lambda_C{}^3 F_q{}^2}{G}, \tag{18}$$

so that the gravitational property of space is

$$G = \frac{\mathrm{dtrd}}{m_a}. \tag{19}$$

In the Primacy of Space ordering, a source mass $M$ first establishes orbital coherence

$$r^3 \mathrm{rson}_{\mathrm{orb}} = \mathrm{dtrd}\frac{M}{m_a}. \tag{20}$$

The radial acceleration follows:

$$a_{\mathrm{orb}} = r\,\mathrm{rson}_{\mathrm{orb}} = \frac{\mathrm{dtrd}}{m_a}\frac{M}{r^2} = \frac{GM}{r^2}. \tag{21}$$

A test mass converts this spatially established acceleration into the Newtonian force representation. The hierarchy is

$$\boxed{\mathrm{dtrd} \longrightarrow \text{Keplerian spatial coherence} \longrightarrow \text{acceleration} \longrightarrow \text{material force.}} \tag{22}$$

### 3.2 Internal, unit-local, and relational geometry

Define

$$\mu_p^{(0)} := \frac{m_p^{(0)}}{m_e}, \qquad \Omega_A := \frac{A_u}{k_C} = 16\pi^2, \qquad \Pi_A := \Pi_{\text{phys}} = \frac{6\pi^3}{16}. \tag{23}$$

The leading balance condition is

$$\boxed{\mu_p^{(0)} = \Omega_A \Pi_A = 6\pi^5.} \tag{24}$$

Its three factors have distinct roles:

$$\begin{aligned} \mu_p^{(0)} &: \text{internal stable-particle mass closure,} \\ \Omega_A &: \text{Aether-unit orientation capacity,} \\ \Pi_A &: \text{relational packing compatibility.} \end{aligned} \tag{25}$$

The balance invariant is

$$\mathfrak{B}_A := \frac{\mu_p^{(0)}}{\Omega_A \Pi_A} = 1. \tag{26}$$

Figure 1 summarizes the closure.

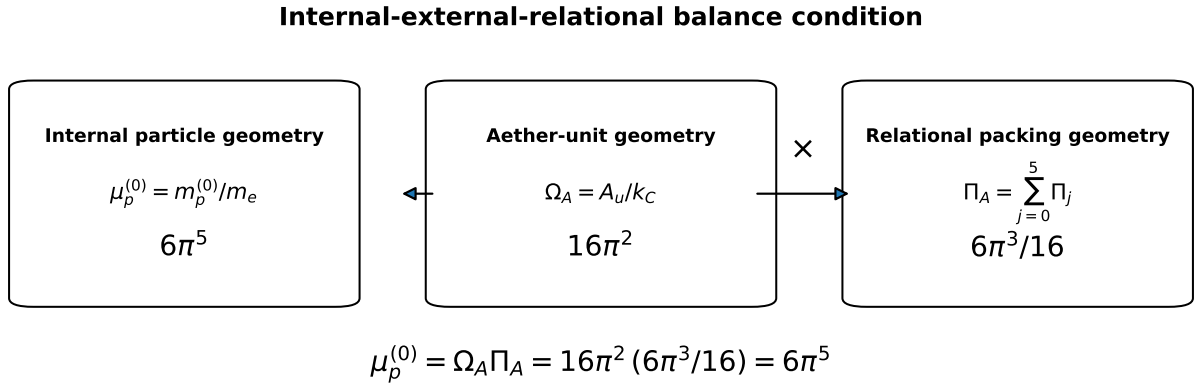


Figure 1: The internal–external–relational balance condition. The leading proton mass geometry is not assigned independently of the Aether Unit or its packing relations.

The complete proton ratio used in APM is

$$\begin{aligned} \mu_p = 6\pi^5 + \pi^{-3} + 2\pi^{-6} + 2\pi^{-8} + 2\pi^{-10} \\ + 2\pi^{-13} + \pi^{-15}. \end{aligned} \tag{27}$$

The leading term is the global balance closure; the inverse powers are local incidence and curvature refinements. This paper uses only the leading equality in deriving the six-port fabric. The dynamical origin of every correction exponent remains a separate proof obligation.

## 4 From Six Packing Components to Six Relational Ports

### 4.1 Reinterpretation of the older six-string language

The earlier packing paper adopted $N_s = 6$ loxodromic strings, each assigned a formal swept-band measure ${\lambda_C}^2/2$, and evaluated the summed packing functional [Thomson III, 2025d]. The later chronogeometry makes literal simultaneous occupation untenable: one Aether Unit can express one occupied Ligamen channel at an exposed moment [Thomson III, 2026a]. The correct interpretation is therefore

$$\boxed{N_s = 6 \text{ counts six formal packing or closure components, not six occupied Ligamens.}} \tag{28}$$

Packing is relational by definition. A node-local Aether quantity can reside on one Unit, but packing exists only between Units. Accordingly, the decomposition

$$\Pi_A = 6\left(\frac{\pi^3}{16}\right) \tag{29}$$

requires six equal edge contributions

$$\Pi_j = \Pi_0 := \frac{\pi^3}{16}, \qquad j = 0, \ldots, 5. \tag{30}$$

Each contribution carries the leading particle-mass increment

$$\Omega_A \Pi_0 = 16\pi^2\left(\frac{\pi^3}{16}\right) = \pi^5, \tag{31}$$

so that

$$\mu_p^{(0)} = \sum_{j=0}^{5} \pi^5 = 6\pi^5. \tag{32}$$

### 4.2 Six equal phase labels

Assign the six relational components equally spaced phase labels

$$\varphi_j = \frac{2\pi j}{6}, \qquad j = 0, \ldots, 5. \tag{33}$$

These phases were already implicit in the six-path construction, where phase-shifted first-, second-, and third-harmonic terms were used to prevent the family from collapsing into only three identical curves. Here the phases are used as relational coordinates rather than material strings.

A six-point phase sample has one constant mode and five nonconstant real Fourier coordinates:

$$\cos\varphi, \quad \sin\varphi, \quad \cos 2\varphi, \quad \sin 2\varphi, \quad \cos 3\varphi. \tag{34}$$

There is no independent $\sin 3\varphi_j$ coordinate because $\sin(\pi j) = 0$ on the six-point set.

## 5 The Regular Five-Dimensional Phase Simplex

Define

$$\boldsymbol{q}_j = \left(\sqrt{\frac{1}{3}}\cos\varphi_j, \sqrt{\frac{1}{3}}\sin\varphi_j, \sqrt{\frac{1}{3}}\cos 2\varphi_j, \sqrt{\frac{1}{3}}\sin 2\varphi_j, \sqrt{\frac{1}{6}}\cos 3\varphi_j\right)^T. \tag{35}$$

Using the cosine difference identities,

$$\boldsymbol{q}_i \cdot \boldsymbol{q}_j = \frac{1}{3}\cos(\varphi_i - \varphi_j) + \frac{1}{3}\cos 2(\varphi_i - \varphi_j) + \frac{1}{6}\cos 3(\varphi_i - \varphi_j). \tag{36}$$

For $i = j$ this equals $5/6$. For every distinct pair it equals $-1/6$. Hence

$$\boxed{\boldsymbol{q}_i \cdot \boldsymbol{q}_j = \delta_{ij} - \frac{1}{6}.} \tag{37}$$

After normalization $\widehat{\boldsymbol{q}}_j = \sqrt{6/5}\,\boldsymbol{q}_j$,

$$\widehat{\boldsymbol{q}}_i \cdot \widehat{\boldsymbol{q}}_j = \begin{cases} 1, & i = j, \\ -1/5, & i \neq j. \end{cases} \tag{38}$$

This is exactly the Gram matrix of a regular 5-simplex. The six equally phased relational components therefore constitute the minimal symmetric reference frame of five-dimensional chronogeometry. The construction is also a finite normalized tight frame [Benedetto and Fickus, 2003].

The vector sum vanishes:

$$\sum_{j=0}^{5} \boldsymbol{q}_j = 0. \tag{39}$$

Thus the six references close without selecting a preferred five-dimensional direction. In affine language, six reference vertices are the minimal simplex frame required to address a destination in five dimensions. The central realized Aether state is not a seventh simplex vertex; it is the state whose relationships to the six references define its local address.

## 6 Antipodal Parity and the Exact $3 + 2$ Split

The antipodal phase translation is

$$\varphi_{j+3} = \varphi_j + \pi. \tag{40}$$

Under this translation,

$$\begin{aligned} \cos(\varphi + \pi) &= -\cos\varphi, & \sin(\varphi + \pi) &= -\sin\varphi, \\ \cos 2(\varphi + \pi) &= +\cos 2\varphi, & \sin 2(\varphi + \pi) &= +\sin 2\varphi, \\ \cos 3(\varphi + \pi) &= -\cos 3\varphi. \end{aligned} \tag{41}$$

The five-dimensional nonconstant phase space therefore separates into the odd sector

$$V_{\text{odd}} = \operatorname{span}\{\cos\varphi, \sin\varphi, \cos 3\varphi\}, \qquad \dim V_{\text{odd}} = 3, \tag{42}$$

and the even sector

$$V_{\text{even}} = \operatorname{span}\{\cos 2\varphi, \sin 2\varphi\}, \qquad \dim V_{\text{even}} = 2. \tag{43}$$

The odd sector reverses when the relationship direction reverses; it has the transformation property required of a spatial outward normal. The even sector is unchanged under reversal; it supplies the two-dimensional hidden temporal registration. The exact decomposition is

$$\boxed{\mathbb{R}^5 = V_{\text{odd}}^{(3)} \oplus V_{\text{even}}^{(2)}.} \tag{44}$$

The temporal dimensions are not straight Cartesian axes. They are represented by phase rotation in a curved two-dimensional plane. Three distinct temporal registrations occur because the six phases form three antipodal pairs, but those three registrations are vectors in one two-dimensional temporal plane:

$$\boldsymbol{t}_j = \begin{pmatrix} \cos 2\varphi_j \\ \sin 2\varphi_j \end{pmatrix}, \qquad \boldsymbol{t}_{j+3} = \boldsymbol{t}_j. \tag{45}$$

The three unique values are separated by 120°.

For every phase component, the squared norms divide as

$$|\boldsymbol{r}_j|^2 = \frac{1}{2}, \qquad |\boldsymbol{s}_j|^2 = \frac{1}{3}, \qquad \left|\boldsymbol{q}_j\right|^2 = \frac{5}{6}, \tag{46}$$

where $\boldsymbol{r}_j$ and $\boldsymbol{s}_j$ are the odd and even parts. Therefore the normalized participation is

$$\frac{|\boldsymbol{r}_j|^2}{|\boldsymbol{q}_j|^2} = \frac{3}{5}, \qquad \frac{|\boldsymbol{s}_j|^2}{|\boldsymbol{q}_j|^2} = \frac{2}{5}. \tag{47}$$

The phase geometry thus reproduces the same 3 : 2 split as the dimension count.

# 7 Octahedral Ports and the External Compatibility Cell

## 7.1 Exact port normals

Extract and normalize the odd part:

$$\boldsymbol{n}_j = \sqrt{2} \begin{pmatrix} \sqrt{1/3}\cos\varphi_j \\ \sqrt{1/3}\sin\varphi_j \\ \sqrt{1/6}\cos 3\varphi_j \end{pmatrix}. \tag{48}$$

The first three vectors are

$$\begin{aligned} \boldsymbol{n}_0 &= \left(\sqrt{\frac{2}{3}}, 0, \frac{1}{\sqrt{3}}\right)^T, \\ \boldsymbol{n}_1 &= \left(\frac{1}{\sqrt{6}}, \frac{1}{\sqrt{2}}, -\frac{1}{\sqrt{3}}\right)^T, \\ \boldsymbol{n}_2 &= \left(-\frac{1}{\sqrt{6}}, \frac{1}{\sqrt{2}}, \frac{1}{\sqrt{3}}\right)^T. \end{aligned} \tag{49}$$

They are mutually orthonormal. The remaining vectors are their opposites:

$$\boldsymbol{n}_{j+3} = -\boldsymbol{n}_j. \tag{50}$$

The exact port Gram matrix, in phase order, is

$$G_{\text{port}} = \begin{pmatrix} 1 & 0 & 0 & -1 & 0 & 0 \\ 0 & 1 & 0 & 0 & -1 & 0 \\ 0 & 0 & 1 & 0 & 0 & -1 \\ -1 & 0 & 0 & 1 & 0 & 0 \\ 0 & -1 & 0 & 0 & 1 & 0 \\ 0 & 0 & -1 & 0 & 0 & 1 \end{pmatrix}. \tag{51}$$

Up to a global spatial rotation, the six ports are

$$\{+\hat{\boldsymbol{x}}, -\hat{\boldsymbol{x}}, +\hat{\boldsymbol{y}}, -\hat{\boldsymbol{y}}, +\hat{\boldsymbol{z}}, -\hat{\boldsymbol{z}}\}. \tag{52}$$

The six outward directions are therefore exactly octahedral, not approximately octahedral and not inserted by choosing a cubic lattice in advance.

## 7.2 The dual compatibility cell

The convex hull of the six port normals is a regular octahedron. Its dual polytope is a cube. The duality has a physical interpretation:

$$\boxed{\text{internal port-direction polytope: octahedron} \quad \longleftrightarrow \quad \text{external compatibility cell: cube.}} \tag{53}$$

This does not redefine the internal Aether Unit as a cube. The internal Unit remains the double-carrier, loxodromic, toroidal-spherical chronogeometry. The cube represents the external relationship domain through which one Unit shares six face interfaces with six nearest neighbors.

Figure 2 shows the phase set, octahedral projection, and cube dual.

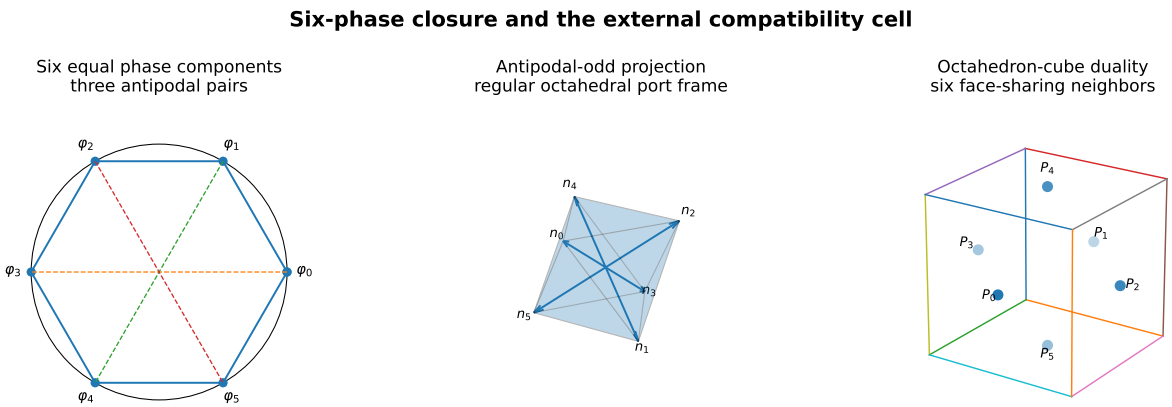


Figure 2: Six equal phases form three antipodal pairs. Their odd projection gives an exact octahedral port frame. The dual external compatibility cell has six faces and six face-sharing nearest neighbors.

The balloon analogy is accurate only if the balloons are deformable and space-filling. Six rigid spheres tangent to one central sphere leave gaps. Six deformable compatibility cells may flatten at their shared interfaces while preserving each Unit's invariant internal area. Each neighboring Unit is complete; the equal quantity $\Pi_0$ is the participation of the shared relation, not the entire surface area of the neighbor.

### 7.3 Neighbor shells and rotational freedom

For a globally aligned six-port graph, the nearest neighbors of Unit $j$ are

$$\boldsymbol{x}_j \pm d_A \boldsymbol{u}_1, \qquad \boldsymbol{x}_j \pm d_A \boldsymbol{u}_2, \qquad \boldsymbol{x}_j \pm d_A \boldsymbol{u}_3. \tag{54}$$

The first shell contains six Units. Higher graph shells satisfy the Manhattan-radius condition $|n_1| + |n_2| + |n_3| = N$ and contain

$$\mathcal{N}_N = 4N^2 + 2 \tag{55}$$

Units. These shells are octahedral at short range.

Macroscopic radial symmetry requires local frame freedom. Let

$$R_j \in SO(3) \tag{56}$$

be the orientation of the local octahedral frame. The actual port normals are

$$\boldsymbol{n}_{j,\alpha} = R_j \boldsymbol{q}_\alpha, \tag{57}$$

where $\boldsymbol{q}_\alpha$ is a fixed reference octahedron. The combination

$$\text{local octahedral discreteness} + \text{continuous frame transport} \tag{58}$$

permits spherical far-field behavior while retaining cubic corrections at quantum-range separation.

### 7.4 Equal packing moments

With equal port weight $\Pi_0$, the first moment vanishes:

$$\sum_{j=0}^{5} \Pi_0 \boldsymbol{n}_j = 0. \tag{59}$$

The second moment is exactly isotropic:

$$\sum_{j=0}^{5} \Pi_0 \boldsymbol{n}_j \boldsymbol{n}_j^T = 2\Pi_0 I_3 = \frac{\Pi_A}{3} I_3. \tag{60}$$

Thus the six-port set has no dipolar bias and reproduces rotational isotropy through second order. Higher moments retain the cubic signature.

## 8 Six-Port State Space and Projectors

Let

$$N = \begin{pmatrix} \boldsymbol{n}_0 & \cdots & \boldsymbol{n}_5 \end{pmatrix} \in \mathbb{R}^{3\times 6}, \qquad T = \begin{pmatrix} \boldsymbol{t}_0 & \cdots & \boldsymbol{t}_5 \end{pmatrix} \in \mathbb{R}^{2\times 6}. \tag{61}$$

The tight-frame identities are

$$NN^T = 2I_3, \qquad TT^T = 3I_2, \qquad NT^T = 0. \tag{62}$$

Define the projectors

$$P_S = \frac{1}{2}N^T N, \qquad P_T = \frac{1}{3}T^T T, \qquad P_0 = \frac{1}{6}\mathbf{1}\mathbf{1}^T. \tag{63}$$

They satisfy

$$P_a^2 = P_a, \qquad P_a P_b = 0 \quad (a \neq b), \qquad P_S + P_T + P_0 = I_6. \tag{64}$$

Therefore

$$\boxed{\mathbb{R}^6 = \mathcal{H}_S^{(3)} \oplus \mathcal{H}_T^{(2)} \oplus \mathcal{H}_0^{(1)}.} \tag{65}$$

The physical interpretation is

$$\begin{aligned} &\mathcal{H}_S : \text{exposed spatial direction,} \\ &\mathcal{H}_T : \text{curved temporal registration,} \\ &\mathcal{H}_0 : \text{common scalar packing participation.} \end{aligned} \tag{66}$$

The nonconstant chronogeometry is $3 + 2 = 5$; the sixth port degree is the equal common mode.

Every continuous unit direction $\widehat{\boldsymbol{k}} \in S^2$ has the exact six-port encoding

$$\boldsymbol{a}_S(\widehat{\boldsymbol{k}}) = \frac{1}{\sqrt{2}}N^T\widehat{\boldsymbol{k}}. \tag{67}$$

Because $NN^T = 2I_3$,

$$|\boldsymbol{a}_S| = 1, \qquad \widehat{\boldsymbol{k}} = \frac{1}{\sqrt{2}}N\boldsymbol{a}_S. \tag{68}$$

Six discrete interfaces can therefore encode a continuously rotating spatial direction without loss. This fact will be essential when the fixed-frame dispersion is interpreted in Section 13.

# 9 Packing-Informed Nearest-Neighbor Compatibility

## 9.1 Profile-level mismatch

For Unit $j$, define the local stretch and logarithmic profile

$$d_j(\theta) = \frac{g_{\eta_j}(\theta)}{g_0(\theta)}, \qquad u_j(\theta) = \ln d_j(\theta). \tag{69}$$

Use the undeformed normalized arc measure

$$\mathrm{d}\mu_0(\theta) = \frac{g_0(\theta)\,\mathrm{d}\theta}{2E(-4)}. \tag{70}$$

The squared logarithmic distance is the minimal local metric that is zero at identity, symmetric, positive, and invariant under common multiplicative stretch. For neighboring Units $j$ and $k$, define

$$\mathcal{E}_{jk} = \frac{\mathrm{enrg}}{2}\Gamma_{jk}\frac{1}{4}\sum_{\sigma,\xi}\int_0^\pi \left[\nu_{j,\sigma,\xi}(\theta) - \nu_{k,\mathcal{T}_{jk}(\sigma,\xi)}(\theta)\right]^2 \mathrm{d}\mu_0. \tag{71}$$

Here $\mathcal{T}_{jk}$ transports the orientation labels of Unit $k$ into the frame of Unit $j$, and $\Gamma_{jk}$ is the fraction of compatible packing participation across the shared interface.

The packing paper now supplies a geometric definition of the latter. If $\Pi_{jk}$ is the registered packing functional on the shared relation, then

$$\boxed{\Gamma_{jk} = \frac{\Pi_{jk}}{\Pi_{\mathrm{phys}}} = \frac{1}{6\pi^5}\frac{A_u}{k_C}\Pi_{jk}.} \tag{72}$$

The previously phenomenological contact coefficient is thus the registered fraction of the complete loxodromic packing invariant.

## 9.2 Small-strain coefficient

Expanding the profile,

$$\nu_\eta(\theta) = b(\theta)\eta + O(\eta^2), \qquad b(\theta) = \frac{4\sin^2\theta\cos 2\theta}{1+4\sin^2\theta}. \tag{73}$$

The first moment is

$$\mathcal{S}_\eta = \int b\,\mathrm{d}\mu_0 = -0.255378263343606\ldots, \tag{74}$$

and the second moment is

$$\mathcal{C}_\eta = \int b^2\,\mathrm{d}\mu_0 = 0.212352156594761\ldots. \tag{75}$$

Since $\varepsilon = \mathcal{S}_\eta\eta + O(\eta^2)$,

$$\boxed{\mathcal{C}_\varepsilon = \frac{\mathcal{C}_\eta}{\mathcal{S}_\eta^2} = 3.25603314631301\ldots.} \tag{76}$$

This coefficient is geometry-only, conditional on the first deformation mode and the full-arc measure.

## 9.3 Carrier character decomposition

The four primitive orientation states admit the discrete character expansion

$$\varepsilon_{\sigma,\xi} = \varepsilon_M + \sigma\varepsilon_E + \sigma\xi\varepsilon_B + \xi\varepsilon_H. \tag{77}$$

The assignments are

$$1 \leftrightarrow M, \qquad \sigma \leftrightarrow E, \qquad \sigma\xi \leftrightarrow B, \qquad \xi \leftrightarrow H. \tag{78}$$

Orthogonality of the four characters gives

$$\frac{1}{4}\sum_{\sigma,\xi}\chi_a\chi_b = \delta_{ab} \tag{79}$$

and therefore diagonalizes the quadratic mismatch.

The nearest-neighbor functional becomes

$$\boxed{\mathcal{E}^{(2)}_{\mathrm{NN}} = \frac{\mathrm{enrg}}{2}\sum_{\langle j,k\rangle}\sum_{a\in\{M,E,B,H\}} K_{a,jk}\left[\varepsilon_{a,j} - s_{a,jk}\varepsilon_{a,k}\right]^2.} \tag{80}$$

In the primitive symmetric limit,

$$K_{a,jk} = \Gamma_{jk}\mathcal{C}_\varepsilon. \tag{81}$$

The sign $s_{a,jk} = \pm 1$ transports the carrier character across the oriented interface.

### 9.4 Sources and graph equation

Add source work:

$$\mathcal{F}[\varepsilon] = \mathcal{E}^{(2)}_{\mathrm{NN}} - \mathrm{enrg} \sum_{j,a} J_{a,j}\varepsilon_{a,j}. \tag{82}$$

Variation gives the covariant weighted graph equation

$$\boxed{\sum_{k\in N(j)} K_{a,jk}\left[\varepsilon_{a,j} - s_{a,jk}\varepsilon_{a,k}\right] = J_{a,j}.} \tag{83}$$

In an aligned unloaded domain, each Unit adopts the weighted mean strain of its neighbors. This is the local mechanics of persistent compatibility in discrete space [Thomson III, 2026d, Chung, 1997].

For the equal six-port graph, with common coefficient absorbed into the source normalization,

$$\Delta_6\varepsilon_j := 6\varepsilon_j - \sum_{\alpha=0}^{5} \varepsilon_{j+\alpha}. \tag{84}$$

The continuum expansion for neighbor spacing $d_A$ is

$$\Delta_6\varepsilon = -d_A^2\nabla^2\varepsilon - \frac{d_A^4}{12}\left(\partial_1^4 + \partial_2^4 + \partial_3^4\right)\varepsilon + O(d_A^6\partial^6\varepsilon). \tag{85}$$

The leading term is isotropic; the first correction retains cubic directionality.

## 10 The Three Source-Injection Laws

### 10.1 Universal definition

For an occupied source Unit, define the dimensionless carrier injection

$$\nu_{a,j} := -\frac{1}{\mathrm{enrg}}\frac{\partial E_{\mathrm{occ},j}}{\partial\varepsilon_{a,j}}. \tag{86}$$

The source term is

$$\mathcal{F}_{\mathrm{src}} = -\mathrm{enrg}\mathcal{N}_{\mathcal{G}}\sum_{j,a}\nu_{a,j}\varepsilon_{a,j}, \qquad J_{a,j} = \mathcal{N}_{\mathcal{G}}\nu_{a,j}. \tag{87}$$

For the canonical six-port Green normalization used below,

$$\mathcal{N}_{\mathcal{G}} = 4\pi. \tag{88}$$

This value fixes the far-field solution $\varepsilon_a = \nu_a\lambda_C/r$ when $d_A = \lambda_C$; the independent geometric derivation of the physical spacing remains open.

### 10.2 Mass injection

The source mass $M$ occupies the fraction $M/m_a$ of the Aether mass capacity. The one-quantum-length coupling to the QMU mass reference is

$$E_{M,q} = \frac{\mathrm{dtrd}}{m_a}\frac{Mm_{\mathrm{e}}}{\lambda_C} = \mathrm{enrg}\frac{M}{m_a}. \tag{89}$$

Positive mass produces inward-compatible spatial organization, so

$$\boxed{\nu_M(M) = -\frac{M}{m_a}, \qquad J_M = -4\pi\frac{M}{m_a}.} \tag{90}$$

The far field is

$$\varepsilon_M(r) = -\frac{M}{m_a}\frac{\lambda_C}{r}. \tag{91}$$

Equation (20) is the primary mass law; the inverse-square force is the later gradient response.

## 10.3 Electrostatic-charge injection

Let the signed electrostatic source measure be

$$Q_E = N_E e^2. \tag{92}$$

The one-quantum-length coupling is $E_{E,q} = k_C Q_E/\lambda_C$. Normalization by Equation (9) gives

$$\nu_E = \frac{k_C}{A_u}\frac{Q_E}{{e_{\mathrm{emax}}}^2} = \frac{Q_E}{16\pi^2{e_{\mathrm{emax}}}^2}. \tag{93}$$

Using Equation (11),

$$\boxed{\nu_E = \frac{\alpha}{2\pi}N_E, \qquad J_E = 2\alpha N_E.} \tag{94}$$

The factor separates into charge strength and geometric projection:

$$\frac{\alpha}{2\pi} = (8\pi\alpha)\left(\frac{1}{16\pi^2}\right). \tag{95}$$

## 10.4 Magnetic-charge injection

Let the signed magnetic-charge measure be

$$Q_B = N_B {e_{\mathrm{emax}}}^2. \tag{96}$$

The full torsional one-quantum-length coupling is $E_{B,q} = A_u Q_B/\lambda_C$. Hence

$$\boxed{\nu_B = \frac{Q_B}{{e_{\mathrm{emax}}}^2} = N_B, \qquad J_B = 4\pi N_B.} \tag{97}$$

There is no $16\pi^2$ reduction because magnetic charge participates through the full distributed loxodromic geometry [Thomson III, 2026b].

For a mass-bearing Ligamen, the common-origin relation gives

$$Q_B = \sigma\xi\frac{m}{m_{\mathrm{e}}}{e_{\mathrm{emax}}}^2, \qquad N_B = \sigma\xi\frac{m}{m_{\mathrm{e}}}. \tag{98}$$

Thus one occupied structure injects

$$\boxed{\boldsymbol{\nu} = \begin{pmatrix} -m/m_a \\ (\alpha/2\pi)N_E \\ \sigma\xi\, m/m_{\mathrm{e}} \end{pmatrix}.} \tag{99}$$

Figure 3 summarizes the source-to-response chain.

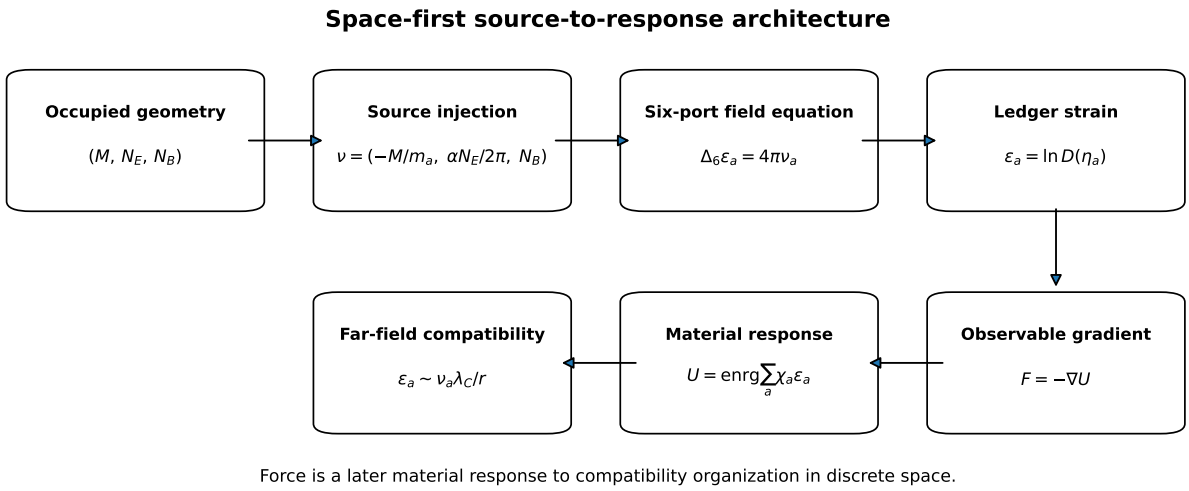


Figure 3: The unified source-to-response architecture. Occupied geometry injects carrier-specific strain into one common six-port compatibility operator.

# 11 Far-Field Interaction and Force Architecture

## 11.1 Continuum Green limit

For slowly varying aligned fields, Equation (83) approaches

$$-\mathcal{K}_a \nabla^2 \varepsilon_a = \rho_a, \tag{100}$$

with

$$\mathcal{K}_a = \frac{\mathrm{enrg} K_a z d_A^2}{6 v_A}. \tag{101}$$

For the six-port graph $z = 6$. A point injection $\mathcal{J}_a \delta^{(3)}(\boldsymbol{r})$ gives

$$\varepsilon_a(r) = \frac{\mathcal{J}_a}{4\pi \mathcal{K}_a} \frac{1}{r}. \tag{102}$$

With the canonical normalization of Section 10,

$$\varepsilon_a(r) = \nu_a \frac{\lambda_C}{r}. \tag{103}$$

The factor $1/(4\pi)$ is the three-dimensional Green factor and is distinct from the internal Aether state-space factor $16\pi^2$.

## 11.2 Test response and pair energy

Let the test-carrier responses be

$$\chi_M = \frac{m_2}{m_e}, \qquad \chi_E = N_{E,2}, \qquad \chi_B = N_{B,2}. \tag{104}$$

The minimal interaction enrg is

$$U_2 = \mathrm{enrg} \sum_{a\in\{M,E,B\}} \chi_a \varepsilon_a. \tag{105}$$

Substituting the source fields gives

$$U_{12}(r) = \frac{\mathrm{enrg}\lambda_C}{r}\left[-\frac{m_1 m_2}{m_a m_{\mathrm{e}}} + \frac{\alpha}{2\pi} N_{E,1}N_{E,2} + N_{B,1}N_{B,2}\right]. \tag{106}$$

Using $\mathrm{enrg}\lambda_C = A_u {e_{\mathrm{emax}}}^2$, Equations (10) and (11), and the QMU pair-square-charge convention,

$$\boxed{U_{12}(r) = -\frac{Gm_1m_2}{r} + \frac{k_C q_{e,12}^2}{r} + \frac{A_u q_{m,12}^2}{r}.} \tag{107}$$

Here $q_{e,12}^2$ and $q_{m,12}^2$ are already signed pair interaction measures. They are not squared again.

The observable static force representation is

$$\boxed{\boldsymbol{F}_{12} = \frac{\widehat{\boldsymbol{r}}}{r^2}\left[-Gm_1m_2 + k_C q_{e,12}^2 + A_u q_{m,12}^2\right].} \tag{108}$$

The inverse-square form follows from three-dimensional compatibility propagation; the coefficients follow from the three source and response channels.

The interaction is therefore unified at the constitutive level:

$$\boxed{\begin{array}{c}\text{occupied geometry} \to \text{carrier source} \to \text{one compatibility operator} \\ \to \text{Ledger strain} \to \text{material response}\end{array}} \tag{109}$$

The present derivation does not yet calculate every absolute edge stiffness directly from the physical contact map. It unifies the architecture, signs, relative carrier strengths, and propagation shape.

### 11.3 Composite cancellation

For a composite source,

$$\nu_M^{\mathrm{tot}} = -\frac{1}{m_a}\sum_i m_i, \qquad \nu_E^{\mathrm{tot}} = \frac{\alpha}{2\pi}\sum_i N_{E,i}, \qquad \nu_B^{\mathrm{tot}} = \sum_i N_{B,i}. \tag{110}$$

Mass injection accumulates with one ordinary sign. Electrostatic and magnetic injections are signed and may cancel. Thus neutral, magnetically closed matter can retain a macroscopic mass-sector deformation while presenting no comparable external charge field.

## 12 Shared-Port Photon Transfer

### 12.1 Antipodal interface rule

Let $\mathcal{A}$ exchange the three opposite port pairs. From the parity decomposition,

$$\boxed{\mathcal{A} = -P_S + P_T + P_0.} \tag{111}$$

Hence a shared interface transforms

$$(\boldsymbol{n}_j, \boldsymbol{t}_j, \Pi_0) \longrightarrow (-\boldsymbol{n}_j, \boldsymbol{t}_j, \Pi_0). \tag{112}$$

The outward normal of Unit $A$ is the inward normal of Unit $B$; the temporal registration and packing participation remain continuous. This is the discrete meaning of the same five-dimensional relationship viewed from opposite spatial sides.

Let $\Psi^{(n)}_{\boldsymbol{x},\alpha}$ be the amplitude leaving Unit $\boldsymbol{x}$ through port $\alpha$ during quantum moment $n$. The shared-face shift is

$$(\mathcal{S}\Psi)_{\boldsymbol{x}+d_A\boldsymbol{n}_\alpha,\,\bar{\alpha}} = \Psi_{\boldsymbol{x},\alpha}, \qquad \bar{\alpha} = \alpha + 3 \pmod 6. \tag{113}$$

If $d_A = \lambda_C$ and one transfer occurs during

$$t_q = \frac{1}{F_q}, \tag{114}$$

then the elementary step rate is

$$\frac{d_A}{t_q} = \lambda_C F_q = c. \tag{115}$$

Equation (115) fixes the causal step scale, not by itself the group rate of a coherent fixed-frame eigenmode.

## 12.2 Temporal phase transport

Represent a temporal state by

$$\boldsymbol{u}(\chi) = \begin{pmatrix} \cos\chi \\ \sin\chi \end{pmatrix}. \tag{116}$$

A photon with freq $f_L$ advances in the curved temporal plane by

$$\delta\chi_0 = 2\pi\frac{f_L}{F_q} \tag{117}$$

per quantum moment. The preliminary Ledger transfer index is selected as

$$\mathfrak{n}_\gamma = \exp(-\varepsilon_\gamma), \tag{118}$$

consistent with $A_u/A_{u0} = \exp(-\varepsilon)$. Across an edge $jk$,

$$\delta\chi_{\gamma,jk} = 2\pi\frac{f_L}{F_q}\exp\left[-\frac{\varepsilon_{\gamma,j}+\varepsilon_{\gamma,k}}{2}\right] + \omega_{jk}, \tag{119}$$

where $\omega_{jk}$ is residual temporal holonomy. This is a constitutive transfer law, not yet the final photon equation.

The carrier-resolved photon strain may be written

$$\varepsilon_\gamma = \varepsilon_M + \zeta^{(\gamma)}_E\varepsilon_E + \zeta^{(\gamma)}_B\varepsilon_B. \tag{120}$$

Mass strain changes the common path phase and trajectory. Electrostatic strain distinguishes temporal-axis participation. Magnetic strain changes handed temporal progression and provides a route to polarization rotation. A complete theory must derive the coefficients $\zeta^{(\gamma)}_E$ and $\zeta^{(\gamma)}_B$ from the physical two-state photon geometry rather than assign them phenomenologically.

### 12.3 Local unitary operator

Define the normalized embeddings

$$E_S = \frac{1}{\sqrt{2}} N^T, \qquad E_T = \frac{1}{\sqrt{3}} T^T, \qquad \boldsymbol{e}_0 = \frac{1}{\sqrt{6}} \mathbf{1}, \tag{121}$$

and the orthogonal matrix

$$Q = \begin{pmatrix} E_S & E_T & \boldsymbol{e}_0 \end{pmatrix}. \tag{122}$$

Let $R_{S,j} \in SO(3)$ transport the local spatial frame, and let $R_{T,j} = R_2(\delta\chi_{\gamma,j})$ rotate the temporal plane. The preliminary through-unit operator is

$$\boxed{\mathcal{C}_j = Q \begin{pmatrix} -R_{S,j} & 0 & 0 \\ 0 & R_{T,j} & 0 \\ 0 & 0 & 1 \end{pmatrix} Q^T.} \tag{123}$$

It is unitary, so an unloaded Aether fabric redistributes port amplitude without creating or destroying phtn. The complete step is

$$\boxed{\Psi^{(n+1)} = \mathcal{U}^{(n)} \Psi^{(n)}, \qquad \mathcal{U}^{(n)} = \mathcal{C}^{(n)} \mathcal{S}.} \tag{124}$$

Discrete unitary propagation has broad mathematical precedent [Aharonov et al., 1993]; the operator here is specialized to the Aether phase and Ledger decomposition.

## 13 Exact Fixed-Frame Lattice Dispersion

### 13.1 Homogeneous Bloch operator

The exact dispersion is calculated for homogeneous undeformed space with a globally fixed port frame. Order the ports as

$$(+\boldsymbol{u}_1, +\boldsymbol{u}_2, +\boldsymbol{u}_3, -\boldsymbol{u}_1, -\boldsymbol{u}_2, -\boldsymbol{u}_3). \tag{125}$$

For Bloch phase vector $\boldsymbol{k}$, define

$$\kappa_a = d_A \boldsymbol{k} \cdot \boldsymbol{u}_a, \qquad D(\boldsymbol{k}) = \operatorname{diag}\left(\mathrm{e}^{i\kappa_1}, \mathrm{e}^{i\kappa_2}, \mathrm{e}^{i\kappa_3}, \mathrm{e}^{-i\kappa_1}, \mathrm{e}^{-i\kappa_2}, \mathrm{e}^{-i\kappa_3}\right). \tag{126}$$

Let the fixed temporal rotation be $R_2(\vartheta)$. Define

$$V_\vartheta = P_S + E_T R_2(\vartheta) E_T^T + P_0. \tag{127}$$

Using $\mathcal{A} D \mathcal{A} = D^{-1}$, the Fourier-space evolution reduces to

$$\boxed{\widehat{\mathcal{U}}(\boldsymbol{k}) = V_\vartheta D(\boldsymbol{k})^{-1}.} \tag{128}$$

The angle $\vartheta$ is an operator parameter independent of the unknown eigenphase. The photon freq is inferred only after the eigenvalue is solved.

## 13.2 Reciprocal characteristic polynomial

Let

$$z = \mathrm{e}^{-i\Omega}, \tag{129}$$

where $\Omega$ is the eigenphase per quantum moment, and define

$$c_a = \cos\kappa_a, \qquad S_1 = c_1 + c_2 + c_3, \qquad S_2 = c_1c_2 + c_2c_3 + c_3c_1, \qquad S_3 = c_1c_2c_3. \tag{130}$$

With $\gamma = \cos\vartheta$, direct evaluation gives

$$\boxed{z^6 - Az^5 + Bz^4 - Cz^3 + Bz^2 - Az + 1 = 0,} \tag{131}$$

where

$$A = \frac{2(\gamma+2)}{3}S_1, \tag{132}$$

$$B = 1 + 2\gamma + 2(1+\gamma)S_2, \tag{133}$$

and

$$C = \frac{4(2\gamma+1)}{3}S_1 + 4(1+\gamma)S_3. \tag{134}$$

At $\boldsymbol{k} = 0$,

$$(z-1)^4\left(z^2 - 2\gamma z + 1\right) = 0. \tag{135}$$

There are four zero-phase modes and one temporal conjugate pair $\Omega = \pm\vartheta$.

Because Equation (131) is reciprocal, set

$$y = z + z^{-1} = 2\cos\Omega. \tag{136}$$

The exact dispersion reduces to the cubic

$$\boxed{y^3 - Ay^2 + (B-3)y + (2A - C) = 0.} \tag{137}$$

Each root $y_r(\boldsymbol{k})$ gives the conjugate phases

$$\Omega_{r,\pm}(\boldsymbol{k}) = \pm\arccos\left[\frac{y_r(\boldsymbol{k})}{2}\right]. \tag{138}$$

The corresponding QMU freq branches are

$$\mathrm{freq}_{r,\pm}(\boldsymbol{k}) = \pm\frac{F_q}{2\pi}\arccos\left[\frac{y_r(\boldsymbol{k})}{2}\right]. \tag{139}$$

## 13.3 Natural three-registration temporal cycle

The three unique temporal registrations are separated by 120°. The minimal cyclic selection is

$$\vartheta_0 = \frac{2\pi}{3}, \qquad \gamma = -\frac{1}{2}. \tag{140}$$

This is a constitutive selection from the temporal triangle, not a separately proven microscopic law. Equations (131) and (137) simplify to

$$\boxed{z^6 - S_1z^5 + S_2z^4 - 2S_3z^3 + S_2z^2 - S_1z + 1 = 0,} \tag{141}$$

$$\boxed{y^3 - S_1 y^2 + (S_2 - 3)y + 2S_1 - 2S_3 = 0.} \tag{142}$$

Along a port axis, $(\kappa_1, \kappa_2, \kappa_3) = (\kappa, 0, 0)$,

$$(y - 2)\left(y^2 - y\cos\kappa - 2\right) = 0. \tag{143}$$

One mode is exactly flat, $\Omega = 0$, and the other roots are

$$y_\pm = \frac{\cos\kappa \pm \sqrt{\cos^2\kappa + 8}}{2}. \tag{144}$$

Along the body diagonal, $\kappa_1 = \kappa_2 = \kappa_3 = \kappa$,

$$(y - 2\cos\kappa)\left(y^2 - y\cos\kappa + \cos^2\kappa - 3\right) = 0. \tag{145}$$

One branch is exactly $\Omega = |\kappa|$ in the principal phase interval.

Figure 4 displays the exact eigenphases along a standard high-symmetry path.

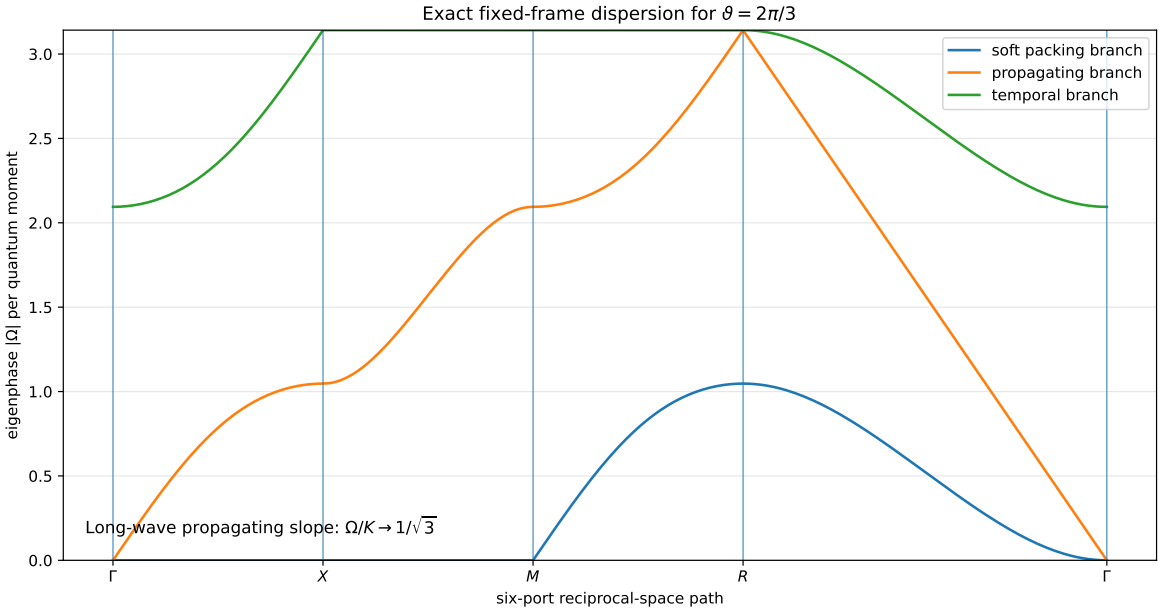


Figure 4: Exact fixed-frame lattice eigenphases for $\vartheta = 2\pi/3$. The three positive branches are a soft packing branch, a linearly propagating branch, and a gapped temporal branch; each has a conjugate negative phase.

## 13.4 Long-wave expansion and the $c/\sqrt{3}$ result

Let

$$K^2 = \kappa_1^2 + \kappa_2^2 + \kappa_3^2, \qquad d_a = \frac{\kappa_a}{K}. \tag{146}$$

Define

$$\mathcal{Q}_4 = d_1^4 + d_2^4 + d_3^4, \qquad \mathcal{Q}_6 = d_1^2 d_2^2 d_3^2. \tag{147}$$

The propagating branch has

$$\boxed{\Omega_\gamma^2 = \frac{K^2}{3} + \frac{7 - 15\mathcal{Q}_4 - 54\mathcal{Q}_6}{216} K^4 + O(K^6).} \tag{148}$$

The leading term is isotropic; the quartic term is cubic-direction dependent. Along a port axis it is $-K^4/27$, along a face diagonal it is $-K^4/432$, and along a body diagonal it vanishes.

The soft packing branch begins as

$$\Omega_P^2 = \frac{1}{4} \frac{\kappa_1^2 \kappa_2^2 \kappa_3^2}{K^2} + O(K^6), \tag{149}$$

and the gapped temporal branch is

$$\Omega_T = \frac{2\pi}{3} + \frac{K^2}{6\sqrt{3}} + O(K^4). \tag{150}$$

The long-wave group rate of the propagating branch is

$$\boxed{v_{\mathcal{U}} = \frac{d_A}{t_q} \lim_{K \to 0} \frac{\Omega_\gamma}{K} = \frac{d_A F_q}{\sqrt{3}}.} \tag{151}$$

If $d_A = \lambda_C$,

$$\boxed{v_{\mathcal{U}} = \frac{c}{\sqrt{3}}.} \tag{152}$$

This result is exact for the fixed-frame operator. Equal coherent participation in three globally locked orthogonal directions distributes the propagation step among those directions. The operator does not yet represent physical free-space photon transport.

### 13.5 Dynamical requirement

Equation (152) identifies the missing mechanism. A photon moving one Aether Unit per quantum moment at $c$ requires the local octahedral frame to parallel-transport so that an outward port aligns with the instantaneous photon direction. The distinction is

$$\begin{aligned} \text{globally fixed port frame} &\longrightarrow v = c/\sqrt{3}, \\ \text{dynamically aligned local frame} &\longrightarrow v = c. \end{aligned} \tag{153}$$

The scalar $6 \times 6$ operator also produces only one linearly propagating conjugate pair. A complete photon operator must supply two degenerate transverse temporal or handed states:

$$\Omega_{\gamma,1}^2 = \Omega_{\gamma,2}^2 = K^2 + O(K^4). \tag{154}$$

Dynamic frame alignment and the two-state photon sector are therefore required results of the dispersion audit, not optional embellishments.

## 14 Predictions and Falsifiable Consequences

The six-port foundation produces a focused set of predictions and internal closure tests.

## 14.1 Balance closure

Independent QMU determinations of the Aether orientation ratio and relational packing functional must satisfy

$$\left(\frac{A_u}{k_C}\right)\Pi_{\text{phys}} = 6\pi^5. \tag{155}$$

The leading proton mass ratio must equal the same product, with the full ratio differing only by the derived incidence corrections of Equation (27).

## 14.2 Port Gram matrix

Any explicit geometric realization of the six relational components must reproduce, after projection, three antipodal orthogonal pairs. Its normalized Gram matrix must be equivalent by permutation and rotation to Equation (51). A candidate packing that fails this test cannot represent the six-port Aether fabric developed here.

## 14.3 Quantum-range cubic correction

The short-range discrete field equation predicts corrections with the operator

$$\partial_1^4 + \partial_2^4 + \partial_3^4, \tag{156}$$

not the fully rotationally invariant $\nabla^4$ alone. Long-range fields are isotropic through second order, but sufficiently short-range compatibility propagation retains a cubic angular signature.

## 14.4 Frame-locked defect mode

A region in which local port frames are locked rather than dynamically transported should support the fixed-frame dispersion of Section 13, including the rate $c/\sqrt{3}$, the soft packing branch, and the gapped $2\pi/3$ temporal branch. The result supplies a discriminating signature for a constrained, crystalline, saturated, or defect-bound Aether neighborhood.

## 14.5 Carrier hierarchy

For elementary carriers, the source magnitudes obey

$$|\nu_M| : |\nu_E| : |\nu_B| = \frac{m_{\text{e}}}{m_a} : \frac{\alpha}{2\pi} : 1. \tag{157}$$

The hierarchy follows from one compatibility operator with three distinct capacity normalizations. It is not three independently selected force laws.

## 14.6 Shared temporal registration

Across an undeformed shared interface,

$$(\boldsymbol{n}, \boldsymbol{t}) \mapsto (-\boldsymbol{n}, \boldsymbol{t}). \tag{158}$$

The temporal phase should therefore be transported continuously while the spatial interface normal reverses. Closed loops can accumulate nonzero holonomy only through transported frame mismatch or carrier deformation, consistent with the earlier 5D-to-4D holonomy program [Thomson III, 2025b].

# 15 Discussion

## 15.1 What has been unified

The exercise produces a genuine structural unification. Mass, electrostatic charge, and magnetic charge share one substrate, one logarithmic Ledger strain, one nearest-neighbor compatibility operator, and one source-to-response architecture. Their differences are encoded by distinct character channels and capacity ratios, not by unrelated propagation laws.

The balance condition deepens this unification. Stable-particle masses are not detached inputs placed into an already existing space. Internal mass closure, the external $16\pi^2$ Aether geometry, and the relational $6\pi^3/16$ packing geometry are mutually constrained. Space exists persistently only when its available internal, unit-local, and relational geometries balance.

The six-port result also reconciles two views of space. Locally, a Unit has an orthogonal Euclidean port frame and a cube-dual external cell. Globally, frame transport and deformation permit radial layering and continuous rotational freedom. The Rubik-cube analogy is therefore useful at the level of overlapping local neighborhoods: the six face positions are direct one-port neighbors, the twelve edge positions are two-port composite relations, and the eight corners are three-port composite relations. No Unit belongs exclusively to one block; the local blocks overlap throughout the fabric.

## 15.2 Why recording the fixed-frame failure matters

A less disciplined treatment could have inferred $c$ from $d_A/t_q$ and stopped. The exact dispersion proves that the elementary step rate and the coherent eigenmode rate are different questions. The locked-frame branch gives $c/\sqrt{3}$. This negative result removes an incorrect model and specifies the necessary next construction.

The correct next operator must make the local frame a dynamical field, derive its transport from compatibility minimization, and carry a two-state photon sector. It should recover $c$ without inserting a compensating numerical factor. The $c/\sqrt{3}$ branch should survive only as a constrained or defect-bound mode.

## 15.3 Relation to earlier packing terminology

The six-string terminology of the older packing paper served as a formal multiplicity count but should not remain the physical ontology. The present work supplies the correction: six equal relational phase components exist simultaneously as compatibility relations; one Ligamen channel is materially occupied at an exposed moment. This distinction permits the packing invariant to retain its value while becoming consistent with the finalized Aether chronogeometry.

### 15.4 Remaining derivations

The following tasks remain open:

1. derive $d_A = \lambda_C$ from the complete physical packing geometry rather than from one Unit per volm alone;
2. calculate the interface map $\Pi_{jk}$ from explicit deformed Aether surfaces;
3. derive the absolute edge stiffness and source normalization from that map;
4. construct the compatibility equation for the local frame field $R_j$;
5. derive the two-state photon sector and its carrier projections;
6. solve the exact dispersion of the frame-aligned operator;
7. obtain an independent numerical or experimental prediction not normalized by already known QMU constants.

## 16 Conclusion

The Aether fabric has been developed as a six-port compatibility geometry constrained by one internal–external–relational balance condition. Six equal loxodromic phase components form a regular five-dimensional simplex. Antipodal parity separates that simplex into three exposed spatial coordinates and two curved temporal coordinates. The spatial projection is an exact octahedral port frame whose dual external cell has six face-sharing nearest neighbors.

The same geometry supports a packing-informed nearest-neighbor functional and three carrier source laws. Mass injection is ordered by the spatial dynamic-domain invariant and Keplerian coherence; electrostatic injection is the radially projected charge sector; magnetic injection is full torsional participation. Their far fields share one graph Green function and produce the familiar inverse-square representations only after material response is introduced.

A preliminary unitary photon-transfer operator preserves temporal registration across a shared port while reversing spatial interface orientation. Its exact fixed-frame dispersion gives $c/\sqrt{3}$, proving that the static cubic frame is not the physical free-space photon mechanism. Dynamic local frame alignment and two transverse temporal states are required.

The result is therefore a completed foundational record of six-port kinematics, balance, source injection, and fixed-frame dynamics. It establishes the mathematical platform for the next paper: the frame-aligned photon operator and the dynamical completion of the force-unification program.

## A Detailed Fourier-Simplex Identities

For $\Delta_{ij} = \varphi_i - \varphi_j = \pi(i-j)/3$, Equation (36) is

$$K(\Delta) = \frac{1}{3}\cos\Delta + \frac{1}{3}\cos 2\Delta + \frac{1}{6}\cos 3\Delta. \tag{159}$$

For $\Delta = 0$, $K = 5/6$. For the five nonzero phase separations,

$$\Delta \in \left\{ \frac{\pi}{3}, \frac{2\pi}{3}, \pi, \frac{4\pi}{3}, \frac{5\pi}{3} \right\}, \tag{160}$$

substitution gives $K = -1/6$. Consequently the $6 \times 6$ Gram matrix is

$$G_Q = I_6 - \frac{1}{6}\mathbf{1}\mathbf{1}^T. \tag{161}$$

Its eigenvalues are 1 with multiplicity five and 0 on the common mode. This is the orthogonal projector onto the hyperplane

$$H = \left\{ \boldsymbol{y} \in \mathbb{R}^6 : \sum_{j=0}^{5} y_j = 0 \right\}, \tag{162}$$

which is five-dimensional. The phase construction is therefore equivalent to the standard regular-simplex vertices $\boldsymbol{e}_j - \mathbf{1}/6$ up to an orthogonal transformation.

# B Port Projectors in Phase Order

The spatial and temporal projector entries are

$$(P_S)_{ij} = \frac{1}{2}\boldsymbol{n}_i \cdot \boldsymbol{n}_j, \qquad (P_T)_{ij} = \frac{1}{3}\boldsymbol{t}_i \cdot \boldsymbol{t}_j. \tag{163}$$

The antipodal operator has matrix elements

$$\mathcal{A}_{ij} = \delta_{i,j+3 \bmod 6}. \tag{164}$$

Direct substitution gives

$$\mathcal{A} = -P_S + P_T + P_0. \tag{165}$$

This identity is the algebraic reason spatial directions reverse and temporal registrations remain unchanged across a shared interface.

# C Deformation-Series Data

The arc response has the expansion

$$D(\eta) = 1 - 0.255378263343606\eta + 0.038445658359014\eta^2 + 0.015738677591680\eta^3 + O(\eta^4). \tag{166}$$

Therefore

$$\ln D(\eta) = -0.255378263343606\eta + 0.005836629306\eta^2 + O(\eta^3), \tag{167}$$

and the local inverse is

$$\eta = -3.915760045147\varepsilon + 0.350437298337\varepsilon^2 + O(\varepsilon^3). \tag{168}$$

Positive $\eta$ produces poleward winding, shorter arc, lower curl, and higher $A_u$. Negative $\eta$ produces the opposite response.

## D Characteristic Polynomial Check

The homogeneous operator is a product of orthogonal or unitary factors, so its eigenvalues lie on the unit circle. The relation

$$\mathcal{A}D(\boldsymbol{k})\mathcal{A} = D(\boldsymbol{k})^{-1} \tag{169}$$

forces the characteristic polynomial to be reciprocal. Expanding $\det[zI_6 - V_\vartheta D^{-1}]$ and collecting the elementary symmetric combinations of $c_a = \cos\kappa_a$ yields Equations (131)–(134). Dividing by $z^3$ and using

$$z + z^{-1} = y, \quad z^2 + z^{-2} = y^2 - 2, \quad z^3 + z^{-3} = y^3 - 3y \tag{170}$$

produces the cubic Equation (137).

The reciprocal form is also a numerical validation requirement: any implementation of the transfer operator must return coefficients symmetric under $z \leftrightarrow z^{-1}$ to numerical precision.

## E Dimensionless Numerical Bridge

The main text does not use SI values. For comparison only, the leading balance value is

$$6\pi^5 = 1836.118108711688\ldots, \tag{171}$$

while Equation (27) gives

$$\mu_p = 1836.15267343\ldots. \tag{172}$$

The recommended proton–electron mass ratio is dimensionless and may be compared using the latest CODATA values [Tiesinga et al., 2023]. Agreement with the complete series is external validation; the measured ratio is not inserted into the count construction.

## F Notation and Epistemic Ledger

Table 2: Principal notation and status.

| Quantity | Meaning | Status |
|---|---|---|
| $A_A = {\lambda_C}^2$ | one physically expressed Aether orientation-state area | derived previously |
| $\Omega_A = 16\pi^2$ | unsigned four-state orientation measure and $A_u/k_C$ ratio | derived previously |
| $\Pi_A = 6\pi^3/16$ | complete six-component relational packing invariant | derived previously |
| $\mu_p^{(0)} = \Omega_A\Pi_A$ | internal–external–relational balance | central identification |
| $\boldsymbol{q}_j$ | five-dimensional six-phase simplex vertex | derived here |
| $\boldsymbol{n}_j$ | three-dimensional outward port normal | derived here |
| $\boldsymbol{t}_j$ | two-dimensional temporal registration | derived here |
| $\Gamma_{jk} = \Pi_{jk}/\Pi_A$ | registered interface participation | derived conditional on $\Pi_{jk}$ |

| Quantity | Meaning | Status |
|---|---|---|
| $\varepsilon = \ln D(\eta)$ | additive Ledger strain | derived previously |
| Squared-log edge metric | nearest-neighbor mismatch measure | constitutive selection |
| $\mathcal{N}_{\mathcal{G}} = 4\pi$ | canonical point-source normalization | selected Green normalization |
| $d_A = \lambda_C$ | neighbor-center spacing | hypothesis requiring packing proof |
| $\vartheta = 2\pi/3$ | temporal cycle of the three registrations | constitutive selection |
| $\widehat{\mathcal{U}}$ | fixed-frame six-port transfer operator | derived conditional model |
| Dynamic $R_j$ law | compatibility-driven local frame alignment | open |
| Two photon branches | transverse temporal or handed states | open |

## Acknowledgments

The Quantum AetherDynamics Institute (QADI) is a private 501(c)(3) research institute developing the Aether Physics Model and Quantum Measurement Units [Thomson III, 2025a]. The author acknowledges the earlier geometric work of Tom Gutman, whose loxodromic and cardioid constructions motivated the continuing search for a realizable Aether geometry.

## Data, Code, and Reproducibility

The source package accompanying this paper contains the complete LaTeX manuscript, bibliography, QADI class and macro files, and the scripts used to generate the phase, port, source-chain, and dispersion figures. The exact characteristic polynomial can be checked independently by constructing Equations (63), (127), and (126) and evaluating $\det[zI_6 - \widehat{\mathcal{U}}(\boldsymbol{k})]$.

## Acknowledgments

The Quantum AetherDynamics Institute (QADI) is a private 501(c)(3) research institute developing the Aether Physics Model (APM) and Quantum Measurement Units (QMU) Thomson III [2025a]. Publications and data are archived with DOIs in the AetherPhysics Zenodo community: zenodo.org/communities/aetherphysics.

## References

Yakir Aharonov, Luiz Davidovich, and Nicim Zagury. Quantum random walks. *Physical Review A*, 48(2):1687–1690, 1993. doi: 10.1103/PhysRevA.48.1687.

John J. Benedetto and Matthew Fickus. Finite normalized tight frames. *Advances in Computational Mathematics*, 18:357–385, 2003. doi: 10.1023/A:1021323312367.

Fan R. K. Chung. *Spectral Graph Theory*, volume 92 of *CBMS Regional Conference Series in Mathematics*. American Mathematical Society, 1997.

Johannes Kepler. *Astronomia Nova*. Heirs of Erasmus Kempfer, Prague, 1609.

Johannes Kepler. *Harmonices Mundi*. Johann Planck, Linz, 1619.

Isaac Newton. *Philosophiae Naturalis Principia Mathematica*. Joseph Streater for the Royal Society, London, 1687.

David W. Thomson III. Quantum aetherdynamics institute (qadi): Community doi overview and citation guide. Zenodo, 2025a. URL https://doi.org/10.5281/zenodo.17479314.

David W. Thomson III. From 5d chronovibration to 4d holonomy: A rigorous derivation in qmu, 2025b. URL https://doi.org/10.5281/zenodo.17374086.

David W. Thomson III. Geometric foundations of particle masses in the aether physics model: Torsion sign reversal, holonomy-derived mass ratios, and closed-system implications for space manipulation, 2025c. URL https://doi.org/10.5281/zenodo.17544759.

David W. Thomson III. Loxodromic packing of aether units and the unity invariant $\mathcal{U} = 6\pi^5$, 2025d. URL https://doi.org/10.5281/zenodo.17352256.

David W. Thomson III. Topological uniqueness of $A_u/k_C = 16\pi^2$ in the aether physics model (qmu), 2025e. URL https://doi.org/10.5281/zenodo.17336682.

David W. Thomson III. The chronogeometry of the aether unit: Orthogonal temporal dimensions, $16\pi^2$ state space, and ledger-one deformation closure, 2026a. URL https://doi.org/10.5281/zenodo.21538113.

David W. Thomson III. Unified electrostatic and magnetic force laws in the aether physics model: Coulomb's constant as radial projection of the aether unit, 2026b. URL https://doi.org/10.5281/zenodo.20585418.

David W. Thomson III. The geometry of the aether unit: Invariant geometry, time-integrated exposure, and the geometric origin of subatomic particle structure, 2026c. URL https://doi.org/10.5281/zenodo.21223750.

David W. Thomson III. Stable matter of the universe: A geometric construction of persistent space and matter in the quantum aetherdynamics framework, 2026d. URL https://doi.org/10.5281/zenodo.21327579.

David W. Thomson III. Primacy of space over matter, 2026e. URL https://quantumaetherdynamics.org/papers/Primacy_of_Space_over_Matter.pdf. Institutional manuscript.

E. Tiesinga, P. J. Mohr, D. B. Newell, and B. N. Taylor. Codata recommended values of the fundamental physical constants: 2022. *Reviews of Modern Physics*, 95:025010, 2023. doi: 10.1103/RevModPhys.95.025010.